PROCEEDINGS OF SPIE

SPIEDigitalLibrary.org/conference-proceedings-of-spie

Performance optimization of InGaAs/InP SPADs for either low noise or high photon detection efficiency applications

Fabio Signorelli, Fabio Telesca, Enrico Conca, Adriano Della Frera, Alessandro Ruggeri, et al.

Fabio Signorelli, Fabio Telesca, Enrico Conca, Adriano Della Frera, Alessandro Ruggeri, Andrea Giudice, Alberto Tosi, "Performance optimization of InGaAs/InP SPADs for either low noise or high photon detection efficiency applications," Proc. SPIE 12089, Advanced Photon Counting Techniques XVI, 120890D (30 May 2022); doi: 10.1117/12.2618831

SPIE.

Event: SPIE Defense + Commercial Sensing, 2022, Orlando, Florida, United States

Performance optimization of InGaAs/InP SPADs for either low noise or high photon detection efficiency applications

Fabio Signorelli*[a], Fabio Telesca[a], Enrico Conca[a], Adriano della Frera[b], Alessandro Ruggeri[b], Andrea Giudice[b], Alberto Tosi[a]
[a]Dipartimento di Elettronica, Informazione e Bioingegneria, Politecnico di Milano, 20133 Milano, Italy; [b]Micro Photon Devices S.r.l., 39100 Bolzano, Italy

ABSTRACT

InGaAs/InP Single-Photon Avalanche Diodes (SPADs) can achieve high photon detection efficiency (PDE) with a thick absorber, but at the expense of higher dark count rate (DCR). PDE and DCR also depend on the electric field inside the structure, which can be tailored in the design phase and influences the overall performance. We present the design and the experimental characterization of two different 10 μm-diameter InGaAs/InP SPADs. The first one is intended for applications where low noise is the key requirement: at 225 K and 5 V excess bias, it features 1 kcps DCR, 25% PDE at 1550 nm and a timing jitter of 100 ps (FWHM). The second device is an InGaAs/InP SPAD optimized for PDE-enhanced applications, having a PDE up to 50% at 1550 nm, with a DCR of 20 kcps and a timing jitter of 70 ps (FWHM) at 225 K. Alternatively, it features a PDE of 37% at 1550 nm, with a DCR of just 3 kcps and a timing jitter of 100 ps (FWHM). When combined with a custom integrated circuit we developed, both devices show an afterpulsing probability as low as few percent with a gating frequency of 1 MHz and hold-off time of few microseconds at 225 K, allowing to achieve a photon count rate towards 1 Mcps.

Keywords: InGaAs/InP, single-photon avalanche diode (SPAD), dark count rate (DCR), detection efficiency, quantum key distribution (QKD), quantum communications, light detection and ranging (LIDAR)

1. INTRODUCTION

The detection of single photons in the short-wavelength infrared (SWIR) range is required by a growing number of applications, from 3D imaging applications, such as light detection and ranging (LIDAR)[1] and non-line-of-sight imaging (NLOS)[2], to quantum optics applications[3], including quantum key distribution (QKD) and quantum computing. Superconductive single-photon detectors show excellent performance for SWIR single-photon detection, but they require complex and bulky cooling solutions to work at cryogenic temperatures. InGaAs/InP single-photon avalanche diodes (SPADs), instead, benefit from the typical advantages of solid-state photodetectors, such as compactness, low cost, and high reliability, together with good overall performance. Moreover, they require moderate cooling solutions, enabling thus the development of compact and portable modules.

Here, we present the design and the experimental characterization of two InGaAs/InP SPADs with 10 μm-diameter active area. Such small devices are suitable for pigtailing with a single-mode optical fiber by means of a single-lens focusing system, preserving high coupling efficiency. One InGaAs/InP SPAD has been optimized for low-noise operation and will be referred to as LN-SPAD, while the second device structure was tailored for high photon detection efficiency (PDE) in the SWIR range, and will be referred to as HE-SPAD.

*fabio.signorelli@polimi.it; phone +39 02 2399 4005;

Advanced Photon Counting Techniques XVI, edited by Mark A. Itzler, Joshua C. Bienfang, K. Alex McIntosh, Proc. of SPIE Vol. 12089, 120890D · © 2022 SPIE
0277-786X · doi: 10.1117/12.2618831

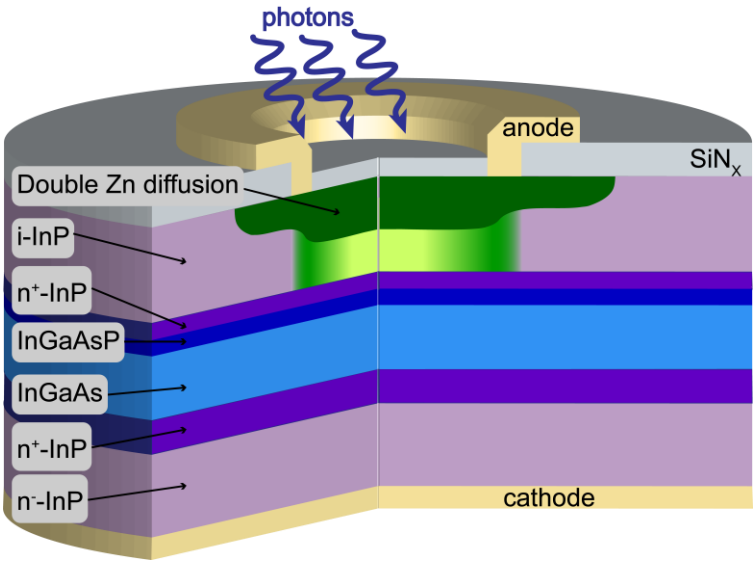

Figure 1. Schematic cross-section of our planar front-illuminated InGaAs/InP SPADs. The main regions of the device are labeled.

2. DEVICE STRUCTURE

Our InGaAs/InP SPADs are front-illuminated planar devices, and they are fabricated as a separate absorption, grading, charge and multiplication (SAGCM) structure. A schematic representation of the cross-section is reported in Figure 1. A double zinc diffusion defines the p-n junction and the active area. The "deep" diffusion guarantees a high electric field inside the multiplication region, while the "shallow" diffusion is needed both for avoiding premature edge breakdown and for increasing the uniformity of electric field in the active area. A highly-doped charge layer (n^+-InP) shapes the electric field along the vertical direction, in order to ensure high electric field for carrier multiplication in the multiplication region and, at the same time, moderately low electric field inside the InGaAs absorption layer (to minimize tunneling generation). Ultimately, five quaternary (InGaAsP) grading layers with varying molar composition facilitate the transit of photogenerated holes from the absorption region to the multiplication region, by reducing the potential barrier (valence side) at the heterointerface.

2.1 Low-noise InGaAs/InP SPAD (LN-SPAD)

Starting from our previous-generation devices[4], we developed a more accurate TCAD model of InGaAs/InP SPADs and

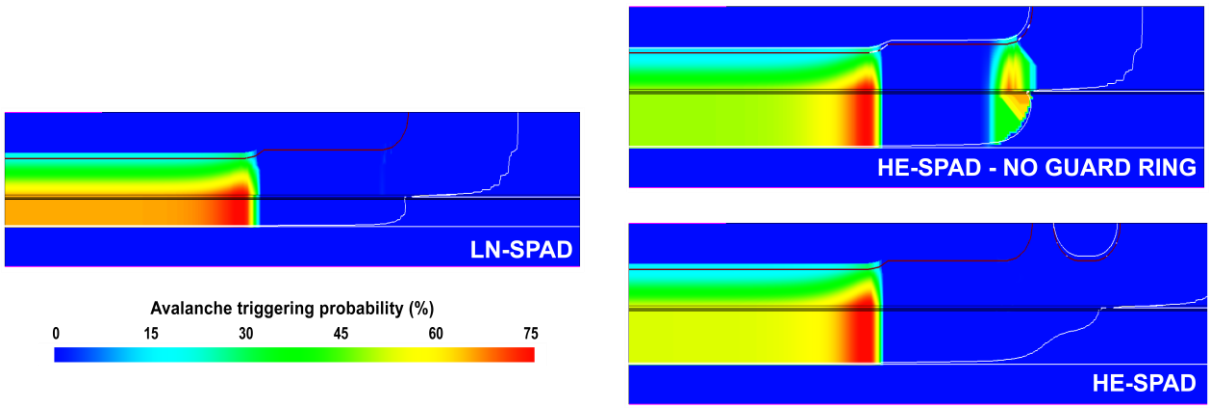

Figure 2. Example of avalanche triggering probability simulations for LN-SPAD and HE-SPAD (without and with guard ring structure).

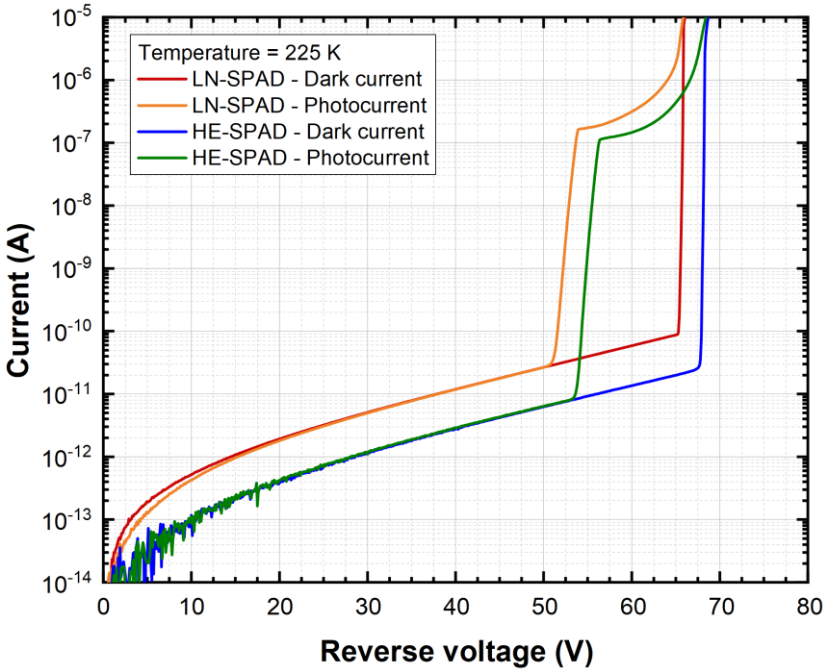

Figure 3. Current-voltage (I-V) characteristics of LN-SPAD and HE-SPAD, measured at a temperature of 225 K. Both dark current and photocurrent (where devices were illuminated with a 1550 nm continuous wave laser) are reported.

we tailored the internal structure to lower the detector noise. We finely tuned the depth of both the shallow and deep diffusions to improve the uniformity of the avalanche triggering probability (i.e., the probability that a photogenerated electron-hole pair can trigger a self-sustained avalanche) inside the active area (see Figure 2). In detail, we reduced the depth difference between the two diffusions (keeping it high enough to avoid edge breakdown), which also helps reducing the charge persistence effect[5] thanks to the enhanced electric field below the shallow diffusion. Our new detector also features a wider shallow diffusion for further reducing the charge persistence effect, thanks to the wider high-field area below the shallow diffusion itself. Moreover, we also tailored the charge layer, by slightly increasing its total amount of charge, with the aim of reducing the electric field inside the InGaAs layer below the multiplication region and, therefore, the noise of the device, but still guaranteeing saturated hole velocity for having low timing jitter.

2.2 High-efficiency InGaAs/InP SPAD (HE-SPAD)

In the high-efficiency device, the thickness of the absorption layer is ~ 2 µm, in order to absorb about 50% more photons than the LN-SPAD structure. However, having a thicker InGaAs layer comes with some disadvantages: i) higher noise due to a bigger active volume; ii) reduced active area uniformity and iii) possible premature edge breakdown (see Figure 2). Therefore, we tailored its internal structure by optimizing the shape and depth of the double zinc diffusion to enhance the uniformity of the active region, and we also added a guard ring (GR) structure with its dedicated bonding pad in order to better control the electric field below the double diffusion and prevent edge breakdown. A TCAD simulation of the structure is reported in Figure 2. We also tuned the charge layer thickness to further reduce the electric field inside the absorption region and consequently reduce field-assisted carrier generation and, thus, the detector noise.

3. EXPERIMENTAL CHARACTERIZATION

Figure 3 shows the current-voltage characteristics of LN-SPAD and HE-SPAD. Both devices show a breakdown voltage, distinguishable in the “dark current” curves, just below 67 V at 225 K, which is a typical operating temperature for such detectors. In the “photocurrent” curves, acquired while illuminating the SPADs with a 1550 nm continuous-wave laser, it is evident the punch-through voltage (~ 51 and 53 V for the two devices), i.e. the voltage at which the depleted region reaches the InGaAs absorption layer. The breakdown voltage and the punch-through voltage of the HE-SPAD are both higher with respect to the LN-SPAD, because of the thicker absorption layer. HE-SPAD shows a lower dark current compared to LN-SPAD, thanks to the guard ring structure that lowers the electric field near the top surface of the device.

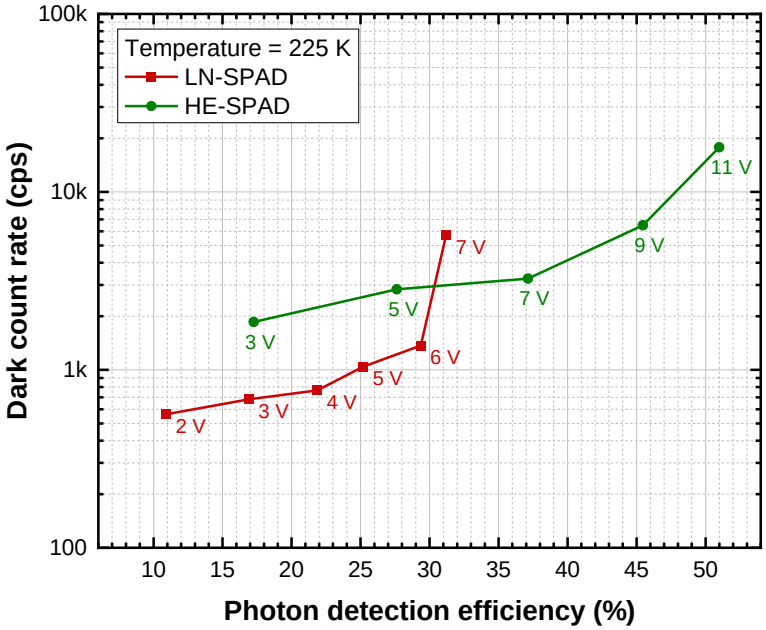

Figure 4. PDE and DCR of the two types of devices, measured focusing a 1550 nm laser inside the SPAD active area. The excess bias voltage corresponding to each measurement point is reported as a label.

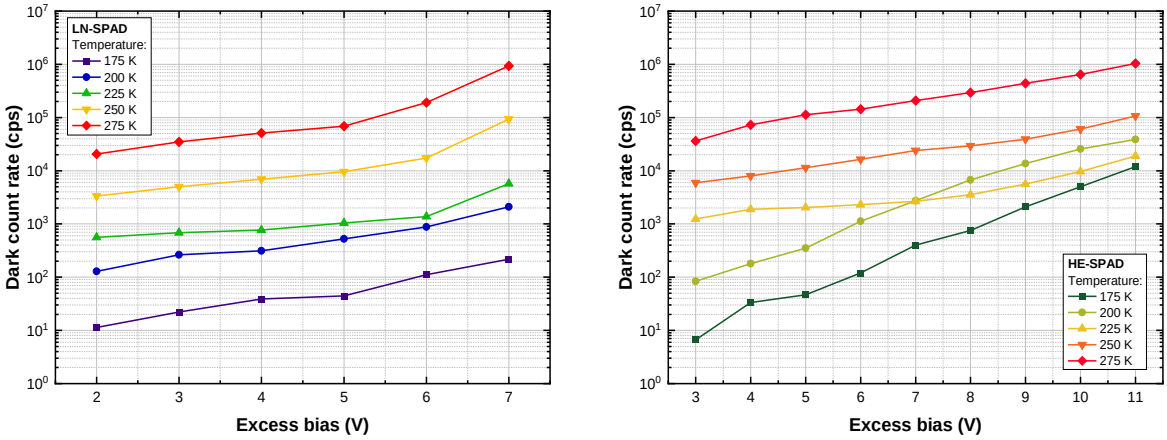

Figure 5. Dark count rate of LN-SPAD (left) and HE-SPAD (right) as a function of the excess bias voltage at different working temperatures.

It is worth noting that, for SPAD operation, the value of the dark current is not important, since it is dominated by surface generation, which does not impair the SPAD noise.

For the experimental characterization in Geiger-mode, we operated the detectors in gated mode with ON-time ranging from 2 to tens of nanoseconds. The SPADs are kept 0.5 V below breakdown voltage during OFF-time, while during ON-time an excess bias voltage (V_{EX}) of few volts is applied above breakdown voltage. For reading the avalanche current, we employed a simple passive quenching circuit, with a 47 kΩ resistor in series to the SPAD that initially quenches the avalanche: the complete quenching is granted by lowering the SPAD voltage at the end of the ON-time.

3.1 Photon Detection Efficiency and Dark Count Rate

We measured the photon detection efficiency of our detectors by focusing a 1550 nm continuous-wave laser inside the active area, with a spot size around 5 µm, thus emulating the spot size attainable with a fiber-pigtailed device. Figure 4 shows the measured PDE and the corresponding dark count rate (DCR) value. The LN-SPAD reaches a PDE just below

30% with a DCR of ~1 kcps, while it features a PDE higher than 10% with a DCR as low as 600 cps. The HE-SPAD reaches a very high PDE above 50% with a DCR below 20 kcps. At V_{EX} = 7 V, this device shows 37% PDE with a low DCR around 3 kcps. Comparing the two presented devices, the LN-SPAD should be the choice when addressing a PDE up to 30%, while if a higher efficiency is required, HE-SPAD shows a lower DCR.

Figure 5 shows the measured dark count rate for the LN-SPAD and the HE-SPAD, at different excess bias voltages and temperatures. At the typical operating temperature of 225 K, easily achievable with a compact multi-stage Peltier cooler inside a small package, the LN-SPAD shows a DCR lower than 1 kcps with $V_{EX} < 5$ V, while the HE-SPAD shows a DCR of few kcps. At even lower temperatures, the DCR of the LN-SPAD decreases towards few tens of cps, while the same decrease is not observed for the HE-SPAD, due to charge persistence effects that are more pronounced as the temperature decreases[5], since the hole lifetime inside the InGaAs layer increases.

3.2 Afterpulsing

To measure the afterpulsing probability (APP) of our devices, we directly wire-bonded them to an integrated read-out circuit we developed specifically for our InGaAs/InP SPADs. This circuit is capable of driving up to 8 SPADs at a maximum excess bias of 5 V and gating frequency up to 100 MHz. A holdoff time is enforced to the SPAD after every avalanche readout by skipping a programmable number of gate periods. A comparator reads the avalanche signal by employing a differential SPAD-DUMMY readout technique, and the resulting quenching time is lower than 2 ns. Figure 6 shows the afterpulsing probability of LN-SPAD and HE-SPAD, calculated with the time-correlated carrier counting (TCCC) technique[6], as a function of the holdoff time. Measurements were performed at different excess bias voltages and different gating frequencies. At 225 K temperature, 1 MHz gating frequency and V_{EX} = 5 V, both devices show an afterpulsing probability of just few percent, thus enabling a maximum count rate towards 1 MHz.

3.3 Timing response

We measured the timing response of our InGaAs/InP SPADs by focusing a 1550 nm pulsed laser (18 ps FWHM) inside the active area and employing a standard TCSPC setup. With the SPAD-DUMMY readout approach, we set a threshold of few mV for achieving low timing jitter. Figure 7 shows the temporal response of LN-SPAD and HE-SPAD at different excess bias voltages. In typical operating conditions, the timing jitter is around 100 ps (FWHM), while it decreases to ~ 70 ps for higher V_{EX}. HE-SPAD shows a slightly worse temporal response with respect to LN-SPAD, due to the increased thickness of the absorption layer.

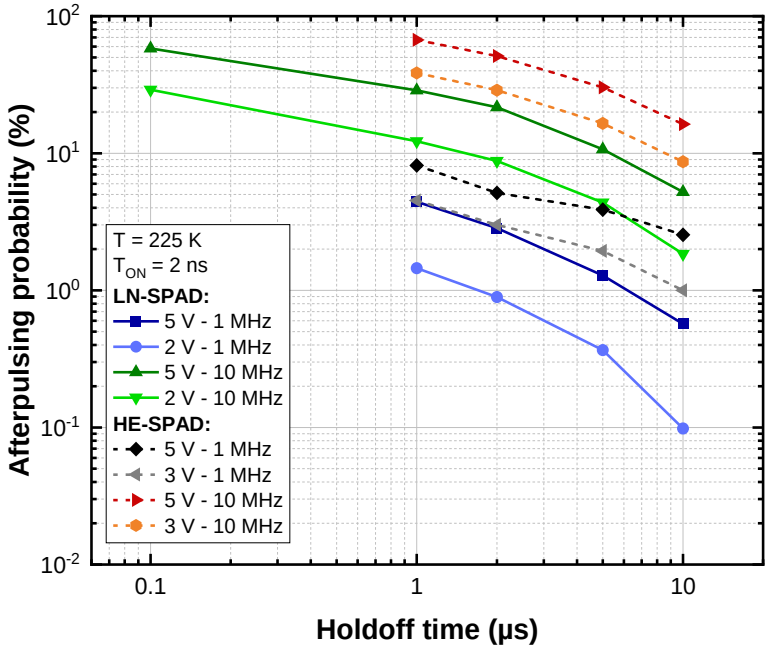

Figure 6. Afterpulsing probability as a function of the holdoff time, measured at different excess bias voltages and gating frequencies for both devices.

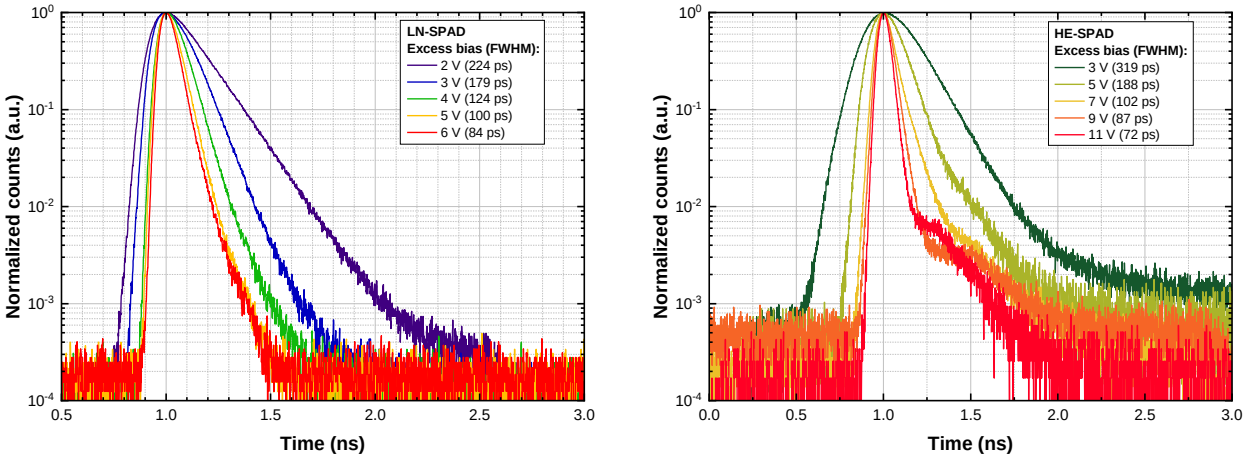

Figure 7. Temporal response of LN-SPAD (left) and HE-SPAD (right) at different excess bias voltages, measured by focusing a 1550 nm pulsed laser inside the active area.

4. CONCLUSIONS

Table 1 shows a performance summary of LN-SPAD, HE-SPAD and InGaAs/InP SPADs from other research groups. The LN-SPAD shows a very low DCR together with a good PDE, with the HE-SPAD achieves state-of-the-art PDE with moderately low DCR, thanks to the newly designed structure. We measured low afterpulsing, despite the low temperature, thanks to the custom integrated circuit we developed. Ultimately, timing response is among the best reported in the literature for InGaAs/InP SPADs. In conclusion, the presented devices are excellent candidates for optical fiber-based quantum applications, where either low noise or high detection efficiency are required, depending on the specific need.

Table 1 – Summary of performance and comparison with state-of-the-art InGaAs/InP SPADs

Ref.	Active area diameter (μm)	Temperature (K)	DCR (cps) @ PDE (%)	APP (%) @ HO (ns)[a]	Timing jitter (ps) @ PDE (%)
LN-SPAD	10	225	560 - 1370 @ 11 - 30	1.4 - 4.4 @ 1000	225 - 84 @ 11 - 30
HE-SPAD	10	225	1.9 k – 18 k @ 17.3 – 51	4.5 – 8.1 @ 1000	319 – 72 @ 17.3 – 51
Baek *et al.*[7]	16	233	100 - 1000[b] @ 10 - 31	2 - 7[c]	N.A.
Fang *et al.*[8]	25	233	260 - 2.5 k @ 7 - 37	4.8 - 12.5 @ < 0.8[c]	N.A.
Park *et al.*[9]	N.A.	253	14.4 k - 16.8 k[d] @ 10.2 - 25.3	0.69 - 21.62 @ 160	N.A.
Tamura *et al.*[10]	9	233	22.2 k - 111.1 k[e] @ 10 - 48[f]	61.5 - 90	450 - 400 @ 10 - 50
Baba *et al.*[11]	12	242	234 k @ 10	86.4 - 25[g] @ 25 - 800	260[h]
Jiang *et al.*[12]	N.A.	253	1.4 k - 3.2 k @ 10 - 25	N.A.	N.A.

[a] HO = hold-off, only reported when available. [b] Computed from dark count probability per gate, with gate frequency = 10 MHz, gate width = 2 ns. [c] Changes with gate signal amplitude. [d] Computed from dark count probability per gate, with gate frequency = 1 GHz, gate width = 400 ps. [e] DCR of the single pixel computed as 1/9th of the DCR of a 3×3 array. [f] Afterpulse probability not subtracted. [g] Measurement conditions: T = 251 K, V_{EX} = 1.9 V. [h] Measurement conditions: T = 255 K, V_{EX} = 1.6 V.

5. ACKNOWLEDGMENT

This work was partially funded by the Autonomous Province of Bozen/Bolzano with the SPIR project (Bando Innovazione 2016).

REFERENCES

[1] Yu, C., Shangguan, M., Xia, H., Zhang, J., Dou, X. and Pan, J.-W., "Fully integrated free-running InGaAs/InP single-photon detector for accurate lidar applications," Opt. Express **25**(13), 14611 (2017).
[2] Wu, C., Liu, J., Huang, X., Li, Z. P., Yu, C., Ye, J. T., Zhang, J., Zhang, Q., Dou, X., Goyal, V. K., Xu, F. and Pan, J. W., "Non–line-of-sight imaging over 1.43 km," Proc. Natl. Acad. Sci. U. S. A. **118**(10) (2021).
[3] Gisin, N. and Thew, R., "Quantum communication," Nat. Photonics **1**(3), 165–171 (2007).
[4] Tosi, A., Calandri, N., Sanzaro, M. and Acerbi, F., "Low-noise, low-jitter, high detection efficiency InGaAs/InP single-photon avalanche diode," IEEE J. Sel. Top. Quantum Electron. **20**(6), 192–197 (2014).
[5] Calandri, N., Sanzaro, M., Tosi, A. and Zappa, F., "Charge Persistence in InGaAs/InP Single-Photon Avalanche Diodes," IEEE J. Quantum Electron. **52**(3) (2016).
[6] Cova, S., Lacaita, A. and Ripamonti, G., "Trapping Phenomena in Avalanche Photodiodes on Nanosecond Scale," IEEE Electron Device Lett. **12**(12), 685–687 (1991).
[7] Baek, S. H., Yang, S. C., Park, C. Y., Park, C. W., Cho, S. B. and Ryu, S. W., "Room temperature quantum key distribution characteristics of low-noise InGaAs/InP single-photon avalanche diode," J. Korean Phys. Soc. **78**(7), 634–641 (2021).
[8] Fang, Y. Q., Chen, W., Ao, T. H., Liu, C., Wang, L., Gao, X. J., Zhang, J. and Pan, J. W., "InGaAs/InP single-photon detectors with 60% detection efficiency at 1550 nm," Rev. Sci. Instrum. **91**(8), 083102 (2020).
[9] Park, C.-Y., Park, C., Han, S.-K., Cho, S.-B. and Baek, S., "Dual anode single-photon avalanche diode for high-speed and low-noise Geiger-mode operation," Opt. Express, Vol. 27, Issue 13, pp. 18201-18209 **27**(13), 18201–18209 (2019).
[10] Tamura, Y., Suzuki, Y., Makino, K., Fujita, T., Nakamura, S., Yamamoto, K., Kurabayashi, T. and Baba, T., "Development of InGaAs MPPC for NIR photon counting applications," Proc. SPIE, Optical Components and Materials XV, p. 105280Z (2018).
[11] Baba, T., Suzuki, Y., Makino, K., Fujita, T., Hashi, T., Adachi, S., Nakamura, S. and Yamamoto, K., "Development of an InGaAs SPAD 2D array for flash LIDAR," Proc. SPIE, Quantum Sensing and Nano Electronics and Photonics XV, p. 105400L (2018).
[12] X. Jiang et al., "InGaAsP/InP Geiger-mode APD-based LiDAR," Proc. SPIE, Optical Sensing, Imaging, and Photon Counting: From X-Rays to THz, p. 107290C (2018).